Synergistic retrievals of ice in high clouds from lidar, Ku-band radar and submillimeter wave radiometer observations

Mircea Grecu[a] and John Yorks [a]

[a] *NASA GSFC*

Corresponding author: Mircea Grecu, mircea.grecu-1@nasa.gov

ABSTRACT: Enter the text of your abstract here.

1. Introduction

The future NASA Atmospheric Observing System (AOS) mission (Braun 2022) is expected to feature new combinations of observations that may be used to quantify the amounts of ice in high clouds and characterize the microphysical properties of ice particles. These observations include lidar backscatter, Ku-band radar reflectivity and submillimeter wave radiometer brightness temperature measurements. While not optimal for cloud ice estimation, but for the characterization of a broader spectrum of cloud and precipitation processes, these observations are nevertheless synergistic from the characterization of ice clouds perspective. That is, despite the fact that lidar observations attenuate quickly in thick ice clouds and the Ku-band radar will not be able to detect clouds characterized by an echo weaker than 8.0 dBZ, the active observations are expected to provide context that may be incorporated into radiometer retrievals. In this study, we investigate the impact of incorporating the lidar and radar observations into the radiometer retrieval of ice clouds. Because the existent amount of coincident backscatter lidar, Ku-band radar, and submillimeter-wave radiometer observations is rather insufficient to derive conclusive results, we employ accurate physical models to simulate the lidar, radar and radiometer observations and use a cross-validation methodology to characterize the retrieval accuracy. As retrievals from passive instrument observations strongly depend on the "a priori" information (Rodgers 2000), for the results to be relevant in real applications it is necessary to base them on realistic vertical distributions of ice properties. Such distributions may be derived from cloud-resolving-model (CRM) simulations (Pfreundschuh et al. 2020) or directly from observations. In this study, we employ the latter approach, as CRMs may still be deficient in properly reproducing the vertical distribution of ice clouds and their associated microphysical properties. Specifically, we use observation and products from the CloudSat (CS) mission (Stephens et al. 2002) to derive a database of ice microphysical properties and associated simulated lidar, radar and radiometer observations. The database is used to investigate the accuracy of the retrieved ice cloud properties from the simulated observations. The article is organized as follows. In Section 2, we describe the approach used to derive the ice properties and the associated simulated observations, the retrieval and the evaluation methodology. In Section 3, we present the results of the evaluation methodology. We conclude in Section 4.

2. Methodology

As previously mentioned, we use CloudSat (CS) observations (Stephens et 2002) to derive the vertical distributions of ice properties needed in the investigation. Although research quality CS cloud ice products exist, to maximize the physical consistency of the approach, we do not use them but derive ice amounts and associated properties directly from CS reflectivity observations. This ensures the consistency between the particle distribution assumptions and the electromagnetic scattering properties used in the CS reflectivity processing and those used the simulation of the lidar, Ku-band radar and radiometer observations. Lidar, Ku-band radar and submillimeter-wave radiometer observations are simulated from CS observations using accurate physical models and realistic assumptions consistent with the most recent knowledge in the field of ice cloud microphysics, and a non-parametric estimation methodology based on the k-Means clustering algorithm MacKay (2003) is used to investigate the instrument synergy. Details of the methodology are presented below.

a. Assumptions and forward models

To quantify the number of ice particles in an elementary atmospheric volume as a function of their size, we use normalized gamma functions (Bringi et al. 2003). The benefit of normalized gamma functions is that they encapsulate the variability of Ice Water Content (IWC) - reflectivity relationship into a single parameter, i.e. the normalized Particle Size Distribution (PSD) intercept (Testud et al. 2001; Bringi et al. 2003). The normalized PSD intercept is defined as $N_w = \frac{4^4}{\pi \rho_w} \frac{IWC}{D_m^4}$, where IWC is the ice water content associated with the PSD, and D_m is the mass weighted mean diameter. Testud et al. (2001) showed that the variability in IWC reflectivity (Z) relationships may be fully explained by variability in N_w, and that a formula of the type

$$IWC = N_w^{1-b} a Z^b \tag{1}$$

perfectly explains the relationships between IWC and Z calculated from observed PSDs. Equation (1) is not sufficient to derive accurate, unbiased estimates of ice water contents, because N_w varies considerably in time and space. Nevertheless, multiple studies showed that it is beneficial to parameterize N_w as a function of various variables, such as temperature (e.g. Hogan et al.

4

2006; Delanoe and Hogan 2008; Deng et al. 2010), rather than using N_w independent relations. In this study, we parameterize N_w as a function of temperature based on the CloudSat 2C-ICE product (Deng et al. 2010; Deng et al. 2013). Specifically, we cluster, based on similarity, a large set 2C-ICE profiles into 18 classes using a k-Means procedure. The mean IWC profiles associated with the 18 classes are shown in continuous lines in Figure 1. Alternative estimates, derived using PSD assumptions and electromagnetic scattering calculations that enable accurate and physically consistent simulations of radar observations at Ku-band and radiometer observations of submillimeter-wave frequencies are also shown in Figure 1. These estimates are based on the self-similarity Rayleigh-Gans approximation (SSRGA) of Hogan et al. (2017). Details regarding the estimation process are provided in the following paragraphs. As apparent in Figure 1, the CS and SSRGA estimates are in good agreement. Some discrepancies due to differences between the SSRGA N_w parameterization and the CS 2C-ICE "a priori assumptions" are also apparent, but they are not deemed critical in this study, whose objective is the investigation of synergistic lidar, Ku-band radar and submillimeter-wave radiometer retrievals, because the outcome is not likely to be sensitive to such details. One may notice that the average IWC profiles in Figure 1 are characterized by different peak values and heights. This facilitates a simple way to reverse-engineer to (some extent) the "a priori" assumptions used in the CS 2C-ICE product and use them in formulation of the type described in Equation (1). Specifically, the derivation of relationships of the type $IWC = a_i Z^{b_i}$ for every class i may be used to study a_i as a function of height. Shown in Figure 2 is a representation of the class multiplicative coefficient a_i as a function of relative height scatter plot. As apparent in the figure, and as expected, a_i exhibits a strong variation with the relative height. Coefficient b_i exhibits a height dependency as well (not shown), but the range of variation is significantly smaller, almost zero relative to the mean value of b. Given that any deviation of the multiplicative coefficient in an IWC-Z relation from an average is equivalent to a deviation of the associated N_w from its mean value (Testud et al. 2001), the variation of a as a function of relative-height may be converted into a N_w as a function of relative-height relationship. We, therefore, use the data in Fig. 2 to parameterize N_w as a function of the relative height.

For the determination of reference a and b values to be used with Equation (1), we assume that PSDs are normalized gamma distributions with $N_w = 0.08 cm^{-4}$ and $\mu = 2$ and calculate
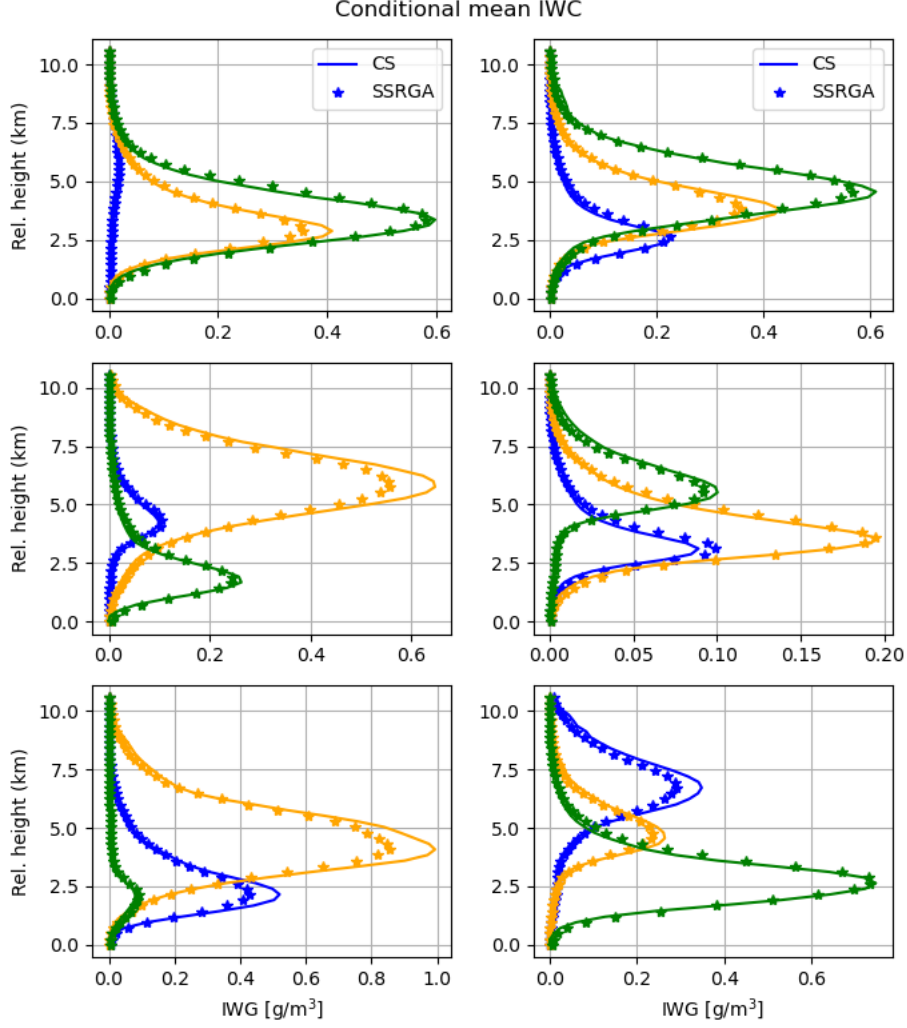
FIG. 1. Mean CS IWC profiles for 18 classes derived using the k-Means clustering algorithm. Associated mean profiles derived from CS reflectivity observations derived using SSRGA scattering calculations and N_w parameterization developed in this study are shown using symbol *. The vertical coordinate is defined relative to the freezing level

$$Z = \frac{\lambda^4}{\pi^5 |K_w|^2} \int_0^\infty N(D, D_m) \sigma_b(D) dD \tag{2}$$

where λ is the radar frequency, $|K_w|$ is the dielectric factor of water, $N(D, D_m)dD$ is the number of ice particles of diameter with D and D+dD per unit volume, D_m is the mass weighted mean diameter of the distribution, and $\sigma_b(D)$ is the backscattering cross-section of ice particle of
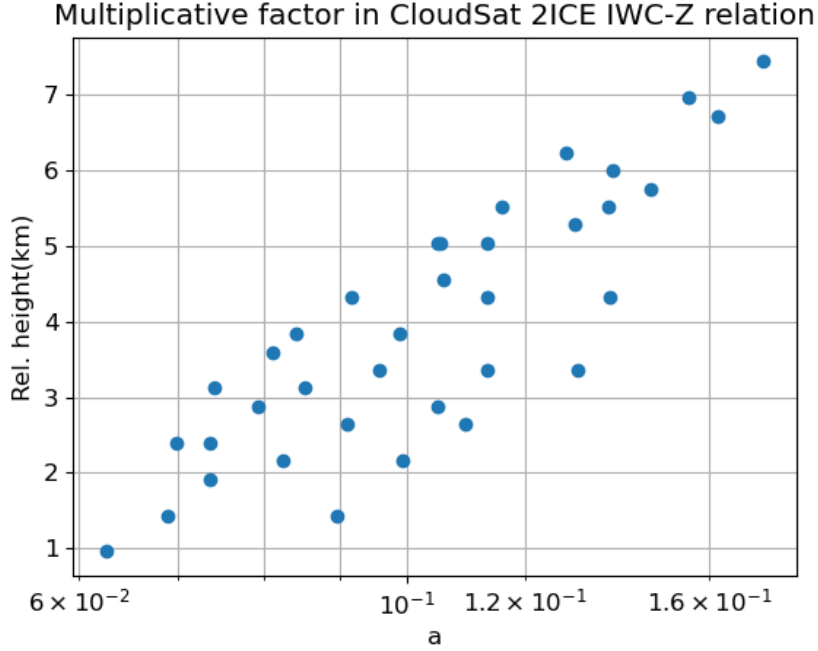
6

Multiplicative factor in CloudSat 2ICE IWC-Z relation

FIG. 2.

diameter D. The mass weighted mean diameter is equidistantly sampled to span the entire range of IWC values in the CS 2C-ICE dataset. The assumed mass-size relation is that of Brown and Francis (1995) because it works well with the SSRGA scattering calculations (Heymsfield et al. 2022). The open source software scatter-1.1 of Hogan (2019) is used to provide the actual scattering properties. The SSRGA theory was developed for millimeter and submillimeter-wave calculations and may not be applicable at lidar's wavelength. Therefore, for lidar calculations, we use the Mie solution included in the scatter-1.1 package. Although more accurate calculations based on more realistic ice particle shapes exist, they are rather incomplete and not readily available. Moreover, Wagner and Deleny (2022) compared lidar backscatter observations with backscatter calculations based on coincident PSD observations and the Mie solution and found good agreement, which suggests that electromagnetic properties derived from Mie calculations are adequate for practical applications. The lidar molecular backscatter and extinction are calculated using the lidar module of the CFMIP Observation Simulator Package (COSP; Bodas-Salcedo et al. 2011). To account for multiple-scattering in the lidar observations, we are using the multiscatter-1.2.11 model (Hogan 2015) of Hogan and Battaglia (2008). Shown in Figure 3 are the distributions of simulated Ku-band radar reflectivity and lidar bacscatter as function of height above the freezing level.
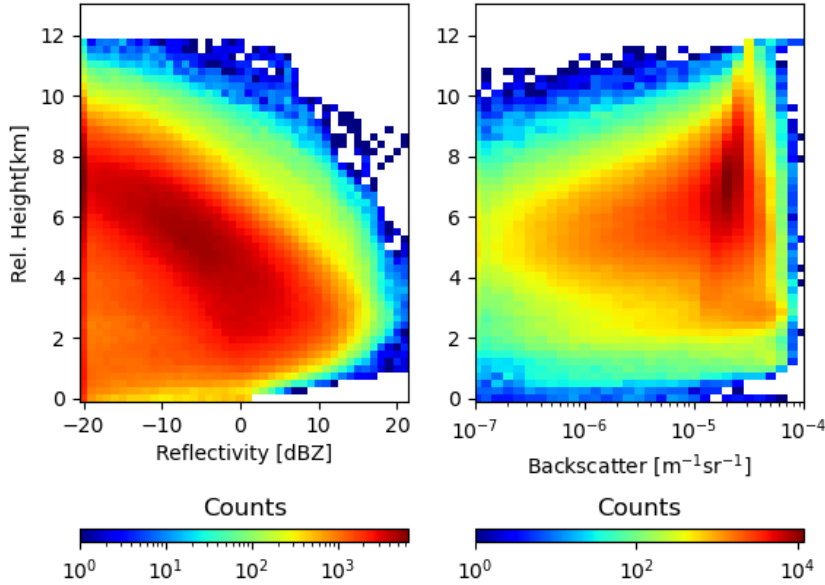
7

Fıg. 3. Simulated distributions of Ku-band radar reflectivity (left) and lidar bacscatter (right) as function of height above the freezing level

The radiometer observations are calculated using a one-dimensional efficient, but accurate, radiative transfer solver based on Eddington's approximation (Kummerow 1993). The Eddington's approximation has been found to work well in cloud and precipitation retrieval application despite its simplicity relative to more general (but also computationally intensive) approaches such as the Monte Carlo radiative transfer solvers (Liu et al. 1996). It should be noted tough that the phase functions of ice particles tend to be highly asymmetric at sub-millimeter wave frequencies. For radiative transfer solutions based on the Eddington's approximation to be accurate it is necessary that the delta-scaling approach (Joseph et al. 1976) be employed. The delta-scaling approach transforms the initial radiative transfer equation into an equivalent one characterized by a less asymmetric scattering function and more extinction, which makes the solution Eddington approximation more stable and accurate. The absorption due to water vapor and other gases is quantified using the Rosenkranz model (Rosenkranz 1998). The water vapor, temperature and pressure distributions are derived based on a WRF simulation of summer convection over the United States. Specifically, the water vapor, temperature and pressure profiles associated with times and areas where the

8

model produces anvils are selected and clustered into 40 classes using the k-Means approach. The mean extinction profiles at the radiometer frequencies are calculated for every class and used in process of calculating the brightness temperatures from the estimated ice profiles using a simple Monte Carlo procedure. That is, given a retrieved ice profile and its scattering property, an anvil class and its associated absorption, temperature and pressure profiles are randomly selected and attached to the ice scattering properties. To make the procedure physically meaningful, temperature rather than height is used in the ice scattering-gas absorption collocation process. The emissivities are randomly chosen between 0.8 and 1.0 and assumed constant for all radiometer frequencies. Brightness temperatures are calculated at 89-, 183.31 ± 1.1, and 325.15 ± 1.5 GHz, which correspond to three of the 10 channels of the SAPHIR-NG radiometer envisioned to be deployed in the AOS mission (Brogniez et al. 2022). The other channels are centered on the same water vapor absorption lines and are not likely to offer additional information in this rather controlled experiment. Nevertheless, the other channels are expected to be useful in reducing the uncertainties caused by variability in the vertical distribution of water vapor, which may be greater in real life than in the simulated environment.

The processing steps used to process the CS reflectivity observations and calculate the lidar, Ku-band and submillimeter-wave radiometer observations may be summarized as follows:

1. Derivation of physically consistent radar and radiometer lookup tables to relate basic radar and radiometer properties (e.g. reflectivity, attenuation, extinction, scattering-albedo, etc.) to PSD parameters such as IWC and D_m. The tables are derived for a single of N_w, but are usable with any value of N_w using the "normalization" operations described in Grecu et al. (2011).

2. Derivation of Nw-relative height parameterization using the 2C-ICE product.

3. Estimation of IWC and related PSD parameters from CS W-band radar observations, using the tables constructed in Step 1 and parameterization derived in Step 2.

4. Calculation of lidar, Ku-band radar and radiometer observations from the estimates derived in Step 3 and the tables obtained in Step 1.

The application of these steps produces a large dataset of approximately 200,000 cloud ice profiles and associated lidar, radar and radiometer observations that may be used to investigate the synergy of the three sensors. Details are provided in the next section.

b. Estimation and evaluation

Given that the lidar observations may attenuate quickly in thick clouds, while the Ku-band radar will not detect clouds with an echo weaker than 8.0 dBZ, the radiometer is the instrument likely to provide by itself the most complete information about the total amount of ice in its observing volume. However, the vertical distribution of ice is difficult to quantify from radiometer-only observations, because significantly different ice vertical distributions may lead to very similar radiometer observations. This makes radiometer-only retrievals highly dependent on the "a priori" information on the distribution of ice clouds in the atmosphere. As previously mentioned, this is the reason why CS-based IWC retrievals were preferred to CRM simulations, as retrievals are expected to exhibit more natural and less biased distributions.

We employ a two-step estimation methodology similar to that of Grecu et al. (2018). In the first step, we estimate from the simulated observations the IWC class, out of the 18 classes of shown in Figure 1, to which the estimated IWC profile is most likely to belong. In the second step, we estimate the IWC profile, using a class specific ensemble Kalman Smoother (EKS) methodology similar to that of Grecu et al. (2018). The EKS algorithm updates the estimated IWC relative to the mean IWC of the class to which the profile belongs based on the differences between the actual active and passive observations and their mean class values. The second step of this procedure is formally identical to the one used in Grecu et al. (2018), but the first step is different. In Grecu et al. (2018), the first step was based on a simple distance-based evaluation. That strategy is likely to be suboptimal in this study, because the joint distribution of IWC profiles and associated observations are significantly more complex. We therefore use a more complex classification methodology based on the TensorFlow library (Abadi et al. 2016). The class estimation model is defined as a TensorFlow Model with two dense layers of 30 neurons each, followed by a softmax layer (Goodfellow et al. 2016). The class estimation model is trained using the 70% of the simulated observations and the corresponding IWC profiles, the remaining 30% of the data being used for evaluation.

$$\mathbf{X} = \bar{\mathbf{X}}_\mathbf{i} + \mathbf{Cov}(\mathbf{X}_\mathbf{i}, \mathbf{Y}_\mathbf{i})\mathbf{Cov}(\mathbf{Y}_\mathbf{i}, \mathbf{Y}_\mathbf{i})^{-1}(\mathbf{Y} - \bar{\mathbf{Y}}_\mathbf{i}) \tag{3}$$

where $\mathbf{X}$ is the state variable describing the IWC profile, $\mathbf{Y}$ is the vector containing the variation, $\mathbf{X}_\mathbf{i}$ is the set of state variables for profiles in class i, and $\mathbf{Y}_\mathbf{i}$ is the set of associated observations. Variables $\bar{\mathbf{X}}_\mathbf{i}$ and $\bar{\mathbf{Y}}_\mathbf{i}$ are the mean values of the state variables and observations in class i, respectively. The covariance matrices between $\mathbf{X}_\mathbf{i}$ and $\mathbf{Y}_\mathbf{i}$ are denoted by $\mathbf{Cov}(\mathbf{X}_\mathbf{i}, \mathbf{Y}_\mathbf{i})$. In step 1, the class is estimated using the TensorFlow model, while in step 2, the IWC profile is estimated using the EKS algorithm summarized in Equation 3.

As already mentioned, a cross validation methodology is used for evaluation, with 70% of the data used for training and the remaining 30% of the data used for validation. The partition of the data into training and evaluation subsets is done randomly. Usually, the partition, training and evaluation steps are repeated several times. However, given the fact that differences in the relationships between the ice property and their associated simulated observations are functions of the meteorological context, and that all regimes are well-sampled in both the training and testing subsets (e.g. out of every 10 pixels in a scene, about 7 end-up in the training dataset, while the others in the testing dataset), the repetition of the partition, training, and evaluation steps multiple times is not necessary. Therefore, in our evaluation, we partition the data into training and evaluation only once and perform all the evaluation for a single partition. The evaluation criteria include the correlation coefficient, the bias, and visual inspections of graphical representations of the estimated properties relative to their references.

3. Results

a. Radiometer-only retrievals

As previously mentioned, submillimeter-wave radiometers are likely to provide by themselves more complete information about the total amount of ice in their observing volumes than lidars or Ku-band radars with limited sensitivity. However, radiometers observations are an integrated measure of radiative process in clouds that provide little information about the vertical distribution of ice. From this perspective, an evaluation in terms of the ice water path (IWP) defined as the vertical integral of the IWC, i.e. $IWP = \int_0^{Z_{top}} IWC(z)dz$ is insightful. Shown in Figure 4 is the
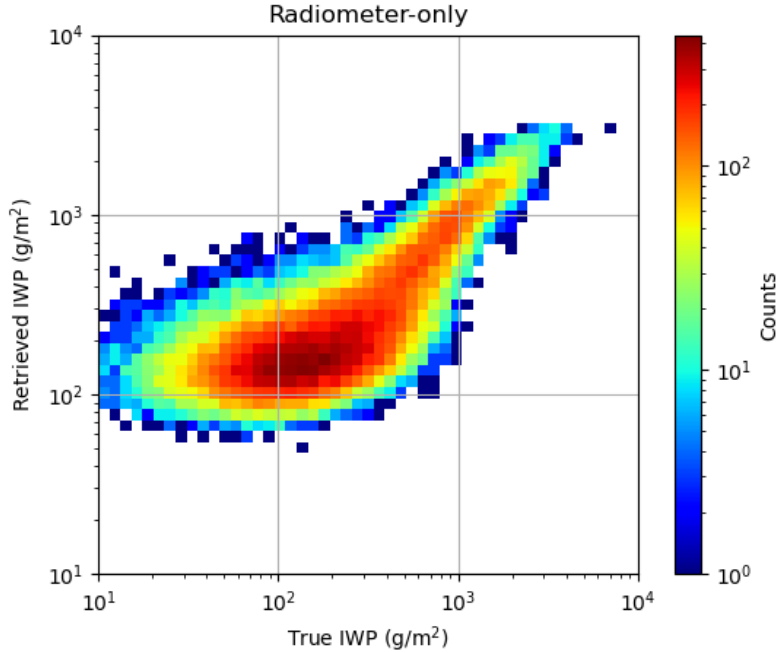
11

FIG. 4. Frequency plot of estimated IWP derived radiometer-observations as a function of the true IWP used in observations synthesis

frequency of IWP estimated from radiometer-only observations as a function of its true value. As apparent in the figure, there is good correlation between the retrieved and the true IWP values. The numerical value of the correlation coefficient is 0.92, and there is no-overall bias. That is, the mean values of retrieved IWP and true IWP values are equal. However, conditional biases are apparent, with overestimation of IWP for values smaller than 100 g/m^2 and some underestimation for values larger than 1000 g/m^2. The biases at the low end of the IWP range are not surprising, given that the impact caused by ice scattering on the total radiometric signal is small for low values of IWP and hard to distinguish from other sources of variability in radiometer observations. Saturation effects are most likely responsible for underestimation at the high end. It should be noted that in this evaluation, only atmospheric profiles that exhibit ice detectable by the CS radar are used. Therefore, a radiometer-only estimation procedure derived from this training dataset is likely to result in significant overestimation if not used in conjunction with a discrimination procedure. However, such procedure is not critical in this study, as the lidar observations may be used to discriminate between clear skies and ice clouds. Although the radiometer-only estimation
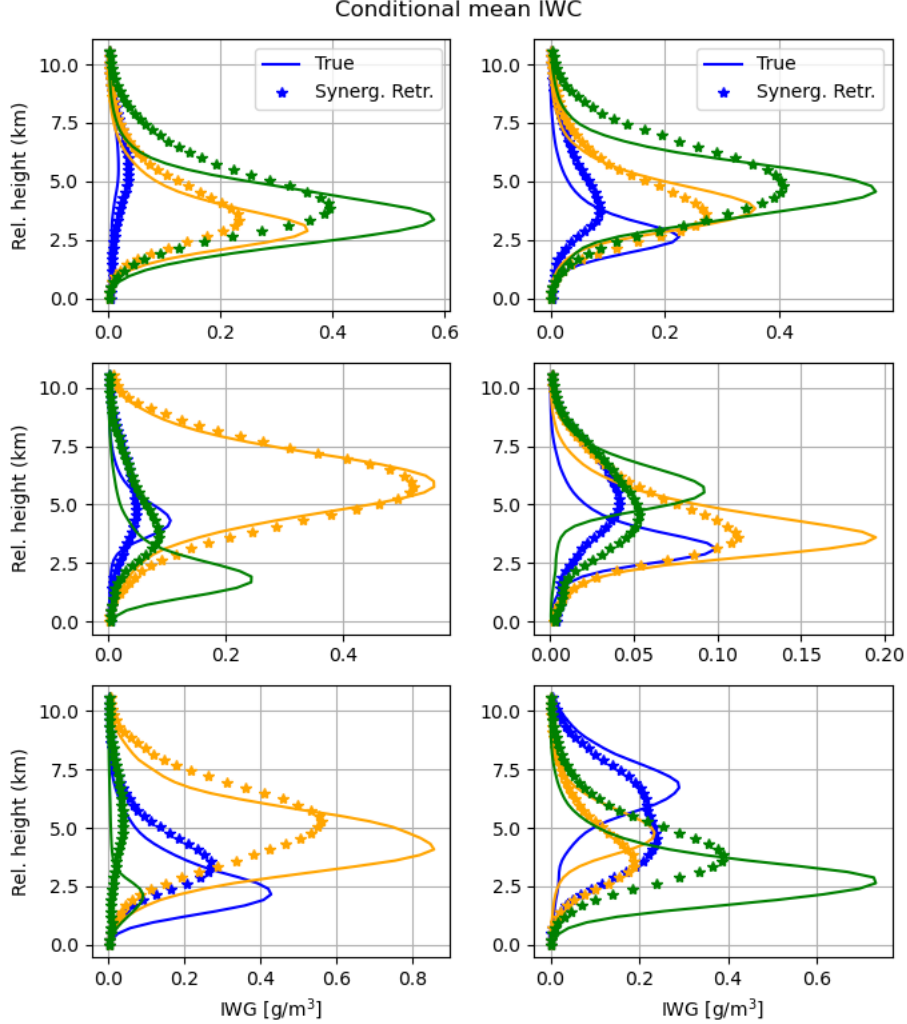
12

FIG. 5. True and radiometer-only retrieved conditional mean IWC for the 18 classes described in Figure 1.

procedure is able to estimate the integrated amount of ice in clouds fairly wells, its ability to characterize the vertical distribution of ice in clouds is limited. Figure 5 shows the conditional vertical distributions of the estimated and true IWC for the 18 classes described in Section 2a and shown in Figure 1.

To express the ability of the radiometer-only methodology to characterize the vertical distribution of ice in clouds in a simple way, we define the ice profile gravity center (GC) as $z_{GC} = \frac{\int_0^{Z_{top}} z IWC(z) dz}{\int_0^{Z_{top}} IWC(z) dz}$, where z is the distance relative to the freezing level, the Z_{top} is the distance from the top of the atmosphere to the freezing level. The IWC is estimated using the kNN regression described in section 2.2 and the estimated z_{GC} is compared to the true z_{GC}. Results are shown in Figure 4. It may
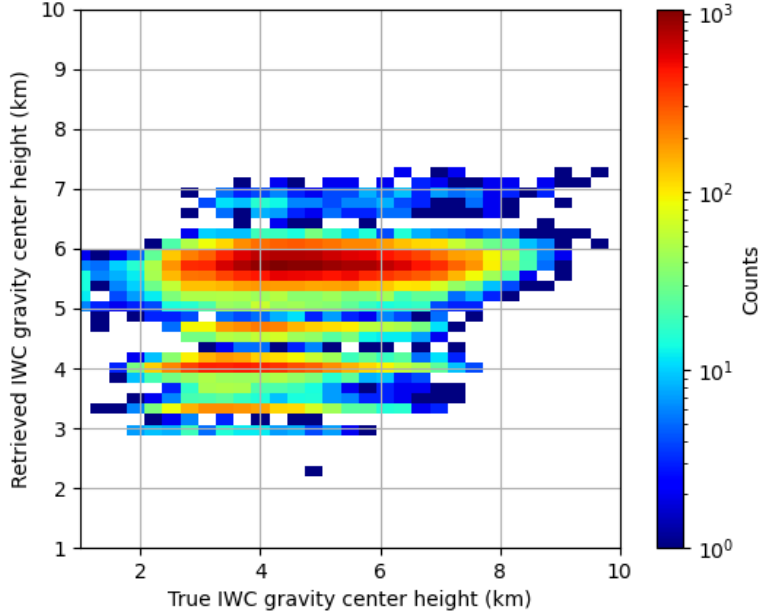
13

FIG. 6. Same as in Figure 3, but for the *IWC* gravity center.

be observed in the figure that while the true *IWC* gravity center exhibits quite a broad distribution, the one retrieved from the radiometer-only observations exhibits a narrow distribution. Moreover, there is almost no correlation between the retrieved and the true IWC gravity center. This is an indication that, while the total amount of ice may be reasonably estimated from radiometer-only observations, its vertical distribution can not be determined from radiometer-only observations.

b. Synergistic retrievals

From the synergy of the instrument perspective, it is useful to investigate how information easily derivable from the active instrument observation can complement the submillimeter-wave radiometer observations. The top of the clouds derived from the lidar backscatter observations is such information. To incorporate it into the *IWC* retrievals, we simply extend the dimension of the input by one entry that contains the lidar-based cloud top estimate. This additional piece of information makes the retrievals more specific by confining the set of potential matches to those that are consistent from the cloud top perspective with the lidar observations.
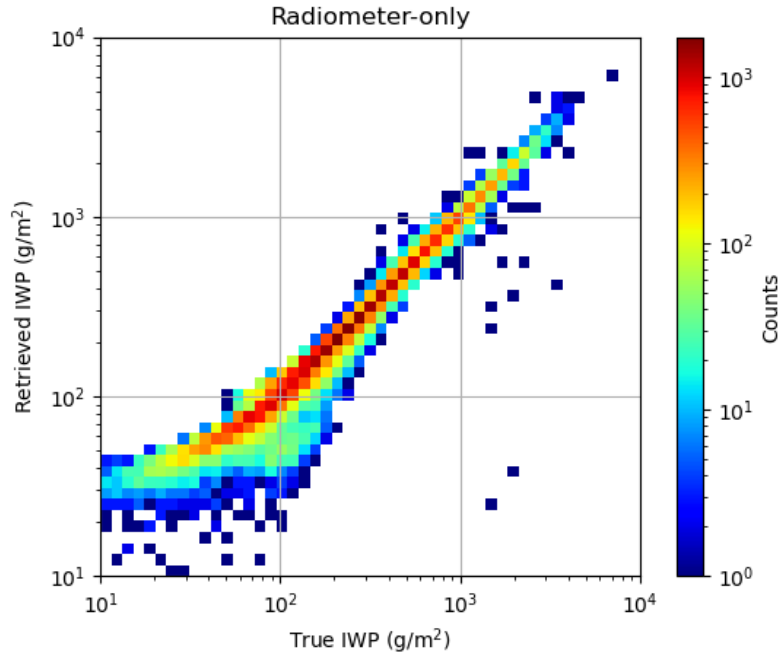
14

Fig. 7. .

Table 1. Performance summary.

Instruments Score	Radiometer	Radar-Radiometer	Lidar-Radiometer	Radar-Lidar-Radiometer
NRMS	0.73	0.59	0.32	0.22
Class. Accurracy	0.39	0.48	0.92	0.94

Shown in Figure 5 is frequency plot of the *IWC* gravity centers estimated from lidar and radiometer observations as a function of the true *IWC* gravity centers. One may note in the figure a significant improvement relative to Figure 4.
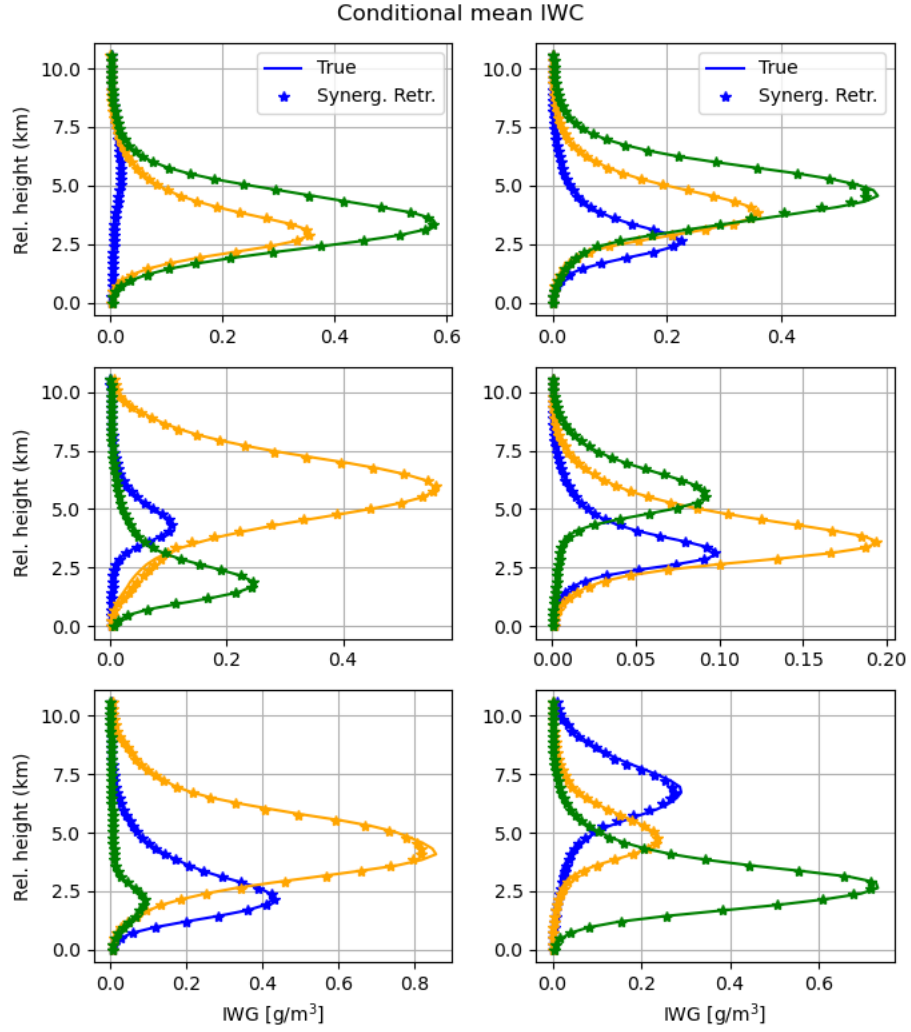
15

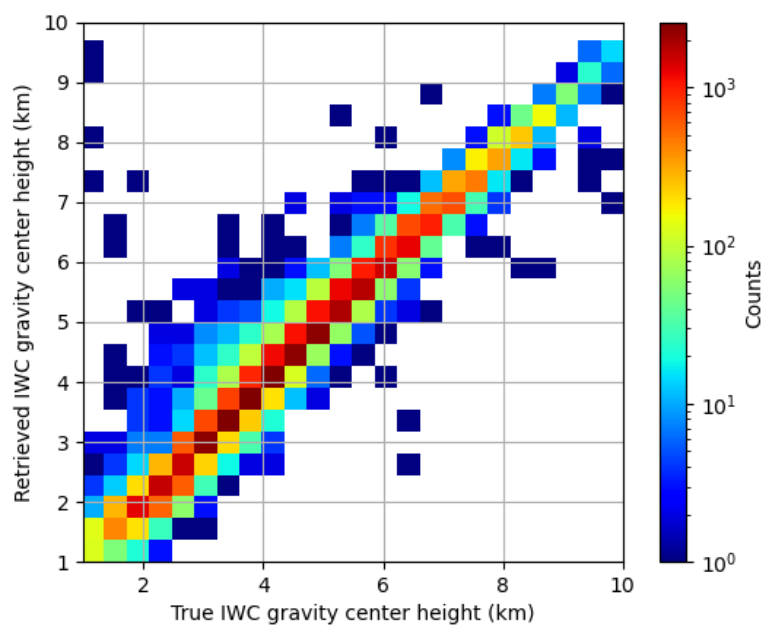Conditional mean IWC

F$_{IG}$. 8. .

FIG. 9. .

Acknowledgments.

Data availability statement.

References

Abadi, M., and Coauthors, 2016: Tensorflow: a system for large-scale machine learning. *Osdi*, Savannah, GA, USA, Vol. 16, 265–283.

Goodfellow, I., Y. Bengio, and A. Courville, 2016: *Deep learning*. MIT press.

Grecu, M., L. Tian, G. M. Heymsfield, A. Tokay, W. S. Olson, A. J. Heymsfield, and A. Bansemer, 2018: Nonparametric methodology to estimate precipitating ice from multiple-frequency radar reflectivity observations. *Journal of Applied Meteorology and Climatology*, **57 (11)**, 2605–2622.

MacKay, D. J., 2003: *Information theory, inference and learning algorithms*. Cambridge university press.